Two-dimensional numerical approach for the vibration isolation analysis of thin walled wave barriers in poroelastic soils

J.D.R. Bordón, J.J. Aznárez, O. Maeso

Instituto Universitario de Sistemas Inteligentes y Aplicaciones Numéricas en Ingeniería,

Universidad de Las Palmas de Gran Canaria, Edificio Central del Parque Científico y Tecnológico del

Campus Universitario de Tafira, 35017 Las Palmas de Gran Canaria, Spain

{jdrodriguez,jaznarez,omaeso}@iusiani.ulpgc.es

Post-print of the paper originally published in Computers and Geotechnics, 71:168-179, 2016.
DOI: http://dx.doi.org/10.1016/j.compgeo.2015.08.007

Abstract

This paper is concerned with the vibration isolation efficiency analysis of total or partially buried thin walled wave barriers in poroelastic soils. A two-dimensional time harmonic model that treats soils and structures in a direct way by combining appropriately the conventional Boundary Element Method (BEM), the Dual BEM (DBEM) and the Finite Element Method (FEM) is developed to this aim. The wave barriers are impinged by Rayleigh waves obtained from Biot's poroelasticity equations assuming a permeable free-surface. The suitability of the proposed model is justified by comparison with available previous results. The vibration isolation efficiency of three kinds of wave barriers (open trench, simple wall, open trench-wall) in poroelastic soils is studied by varying their geometry, the soil properties and the frequency. It is found that the efficiency of these wave barriers behaves similarly to these in elastic soils, except for high porosities and small dissipation coefficients. The efficiency of open trench-wall barriers can be evaluated neglecting their walls if they are typical sheet piles. This does not happen with walls of bigger cross-sections, leading in general to efficiency losses. Likewise, increasing the burial depth to trench depth ratio has a negative impact on the efficiency.

Keywords: vibration isolation, poroelasticity, Rayleigh waves, thin structures, Dual Boundary Element Method, BEM-FEM coupling

1 Introduction

The vibrations induced by machinery or vehicles can travel through the soil to nearby constructions, which can annoy people or cause the malfunction of devices located inside of these. In order to reduce the vibrations, a wave barrier can be installed at a point of the transmission path. The design of each vibration isolation system depends on the source of vibrations, the properties of the transmission path, and the isolation requirements. An open trench is a very efficient system because its stress-free boundaries act as perfect reflectors of elastic waves. Its efficiency greatly depends on the ratio between the Rayleigh wavelength and the trench depth. However, for soil stability reasons, especially in water saturated soils, a pure open trench can not be excavated to any desired depth. Thus, other systems such as in-filled trenches, or the installation of sheet piles or rows of piles, are often used. Another option is reinforcing the open trench by installing retaining sheet piles or concrete walls on both sides of the trench. This type of wave barrier is called an open trench-wall.

There exist a vast literature about the design and analysis of wave barriers. Before the numerical computing era, only experimental studies were performed in order to assess these problems, where the works by Barkan [6] and Woods [34] blazed a trail. Nowadays, analytical, semi-analytical and numerical methods, mainly the Boundary Element Method (BEM), are being used, although experimental methods are still being used to confirm and/or parametrize mathematical models, e.g. [22]. Three kinds of wave barriers in elastic soils have been extensively studied: open and in-filled trenches, and rows of piles. The open and in-filled trenches have been studied through two-dimensional BEM models by Emad et al. [19], Beskos et al. [8, 26], and even formulas for a simplified design have been given by Ahmad et al. [2]. They were studied in three-dimensional problems using BEM models by Banerjee et al. [5] and Dasgupta et al. [15]. The vibration isolation produced by rows of piles have been studied by Avilés et al. [4] analytically, and by Kattis et al. [24] using a three-dimensional BEM model. The open trench-wall systems have been rarely studied, to the authors' knowledge only Tsai et al. [33] using a two-dimensional multidomain BEM model. When compared with elastic soils, much less works dealing with the efficiency of wave barriers in poroelastic soils exist. Cai et al. [12, 11] and Xu et al. [35] studied the isolation efficiency of rows of piles in poroelastic soils using semi-analytical methods, and Cao et al. [13] did the same for open trenches under a moving load. As it is seen, the BEM has been widely applied to study these types of problems because of its own capability to deal with unbounded regions. The Finite Element Method (FEM) has been used also, but mainly in combination with the BEM, being the FEM used for structural parts of the problem. Among other coupled BEM-FEM models used in this field, those developed for the study of the isolation of vibrations produced by moving loads (trains) are of great interest nowadays. To this end, the models developed by Andersen et al. [3] and François et al. [20] are great exponents.

The aim of this paper is twofold. Firstly, to present a two-dimensional BEM-FEM dynamic model for soil-structure interaction analyses, where the structures are thin, and one or both of their faces can interact with the surrounding media. The initial idea of this model for fluid-structure analyses has already been presented [10]. Here, the model is expanded by considering a Biot's poroelastic surrounding medium. Secondly, to apply the proposed model to study a problem of interest where there are clear advantages of its use: the efficiency of thin walled wave barriers buried in this medium. For this study, three kinds of wave barriers are considered: open trench, simple barrier (thin in-filled trench), and open trench-wall; which are impinged by a Rayleigh incident wave field assuming a permeable free-surface.

The rest of the paper is organized as follows. The Biot's poroelasticity model is briefly described in Section 2.1. In Section 2.2, the Rayleigh waves on a permeable free-surface are discussed for this model. In section 2.3, the conventional BEM and the Dual BEM for the Biot's poroelasticity are presented. The soil-structure coupling conditions are described in Section 2.4. In Section 3.1, results obtained from the proposed model are compared with published results. In Section 3.2, a study of the previously mentioned wave barriers under incident Rayleigh waves is presented.

2 Methodology

2.1 Biot's poroelasticity

A very general representation of soils can be done by the Biot's poroelasticity model [9]. This model is able to represent a two-phase medium consisting of a solid frame saturated by a fluid. Let u_i and τ_{ij} be the displacements and stresses of the solid phase, U_i and τ the displacements and equivalent stress of the fluid phase, and $i, j \in [1,2]$. The governing equations in the time domain can be written as:

$$\mu\nabla^2\mathbf{u}+\nabla\left[\left(\lambda+\mu+Q^2/R\right)(\nabla\cdot\mathbf{u})+Q(\nabla\cdot\mathbf{U})\right]+\mathbf{X}=\rho_{11}\ddot{\mathbf{u}}+\rho_{12}\ddot{\mathbf{U}}+b\left(\dot{\mathbf{u}}-\dot{\mathbf{U}}\right) \tag{1}$$

$$\nabla\left[Q(\nabla\cdot\mathbf{u})+R(\nabla\cdot\mathbf{U})\right]+\mathbf{X}'=\rho_{12}\ddot{\mathbf{u}}+\rho_{22}\ddot{\mathbf{U}}-b\left(\dot{\mathbf{u}}-\dot{\mathbf{U}}\right) \tag{2}$$

and the stress-strain relationships as:

$$\tau_{ij}=\delta_{ij}\left[\left(\lambda+Q^2/R\right)(\nabla\cdot\mathbf{u})+Q(\nabla\cdot\mathbf{U})\right]+\mu\left(u_{i,j}+u_{j,i}\right) \tag{3}$$

$$\tau=Q(\nabla\cdot\mathbf{u})+R(\nabla\cdot\mathbf{U}) \tag{4}$$

where $\mathbf{X}$ and $\mathbf{X}'$ are the body forces of the solid and fluid phases, respectively, λ and μ are the Lamé's parameters of the solid phase, Q and R are the Biot's coupling parameters, b is the dissipation constant, and $\rho_{11}=(1-\phi)\rho_\mathrm{s}+\rho_\mathrm{a}$, $\rho_{12}=-\rho_\mathrm{a}$, $\rho_{22}=\phi\rho_\mathrm{f}+\rho_\mathrm{a}$, being ϕ the porosity, ρ_s the solid phase density, ρ_f the fluid phase density, and ρ_a the additional aparent density. In the following, in order to avoid confusion, the subscripts 1 and 2 are used to denote solid phase and fluid phase variables, respectively, while x, y are used to denote coordinates.

Using the Helmholtz decomposition:

$$u_x=\frac{\partial\varphi_1}{\partial x}+\frac{\partial\psi_1}{\partial y},\quad u_y=\frac{\partial\varphi_1}{\partial y}-\frac{\partial\psi_1}{\partial x},\quad U_x=\frac{\partial\varphi_2}{\partial x}+\frac{\partial\psi_2}{\partial y},\quad U_y=\frac{\partial\varphi_2}{\partial y}-\frac{\partial\psi_2}{\partial x} \tag{5}$$

and considering null body forces, two decoupled sets of two equations are obtained from Eqs. (1-2):

$$\varphi_1,\varphi_2\begin{cases}\left(\lambda+2\mu+Q^2/R\right)\nabla^2\varphi_1+Q\nabla^2\varphi_2=\rho_{11}\ddot{\varphi}_1+\rho_{12}\ddot{\varphi}_2+b(\dot{\varphi}_1-\dot{\varphi}_2) & (6)\\ Q\nabla^2\varphi_1+R\nabla^2\varphi_2=\rho_{12}\ddot{\varphi}_1+\rho_{22}\ddot{\varphi}_2-b(\dot{\varphi}_1-\dot{\varphi}_2) & (7)\end{cases}$$

$$\psi_1,\psi_2\begin{cases}\mu\nabla^2\psi_1=\rho_{11}\ddot{\psi}_1+\rho_{12}\ddot{\psi}_2+b(\dot{\psi}_1-\dot{\psi}_2) & (8)\\ 0=\rho_{12}\ddot{\psi}_1+\rho_{22}\ddot{\psi}_2-b(\dot{\psi}_1-\dot{\psi}_2) & (9)\end{cases}$$

The first set is related with a rotational-free (P) displacement field due to scalar potentials φ_1 and φ_2, and the second set with a divergence-free (S) displacement field due to scalar potentials ψ_1 and ψ_2. In the time harmonic regime, these equations lead to the three well known bulk modes of wave propagation in Biot's poroelasticity. Onwards, the circular frequency is denoted as ω, and the assumed time harmonic term is $\exp(i\omega t)$, which is omitted for brevity. If only the time harmonic potentials $\varphi_i=P_i\exp(-ik_\mathrm{P}x)$ are considered, then the bulk P mode is obtained from:

$$P_1,P_2\begin{cases}\left[\omega^2\hat{\rho}_{11}-k_\mathrm{P}^2\left(\lambda+2\mu+Q^2/R\right)\right]P_1+\left[\omega^2\hat{\rho}_{12}-k_\mathrm{P}^2Q\right]P_2=0 & (10)\\ \left[\omega^2\hat{\rho}_{12}-k_\mathrm{P}^2Q\right]P_1+\left[\omega^2\hat{\rho}_{22}-k_\mathrm{P}^2R\right]P_2=0 & (11)\end{cases}$$

where $\hat{\rho}_{11}=\rho_{11}-ib/\omega$, $\hat{\rho}_{22}=\rho_{22}-ib/\omega$ and $\hat{\rho}_{12}=\rho_{12}+ib/\omega$. The wavenumbers k_P are obtained from its characteristic equation:

$$\begin{aligned}&k_\mathrm{P}=\pm\frac{1}{\sqrt{2}}\left(a_1\pm\left(a_1^2-4a_0\right)^{1/2}\right)^{1/2}\\ &a_1=\omega^2\left(\frac{\hat{\rho}_{22}}{R}+\frac{\hat{\rho}_{11}+\hat{\rho}_{22}Q^2/R^2-\hat{\rho}_{12}2Q/R}{\lambda+2\mu}\right),\quad a_0=\omega^4\frac{\hat{\rho}_{11}\hat{\rho}_{22}-\hat{\rho}_{12}^2}{R(\lambda+2\mu)}\end{aligned} \tag{12}$$

where two of the solutions are relevant incoming waves ($\mathrm{Re}(k_\mathrm{P})>0$). Hence, two P modes exist: the wavenumber associated with the fastest wave speed is $k_{\mathrm{P}1}$, while the wavenumber associated with the slowest wave speed is $k_{\mathrm{P}2}$. If only the time harmonic potentials $\psi_i=S_i\exp(-ik_\mathrm{S}x)$ are considered, then the bulk S mode is obtained from:

$$S_1,S_2\begin{cases}\left[\omega^2\hat{\rho}_{11}-k_\mathrm{S}^2\mu\right]S_1+\omega^2\hat{\rho}_{12}S_2=0 & (13)\\ \omega^2\hat{\rho}_{12}S_1+\omega^2\hat{\rho}_{22}S_2=0 & (14)\end{cases}$$

and the wavenumber k_S is obtained from its characteristic equation:

$$k_S=\pm\omega\left(\frac{\hat{\rho}_{11}-\hat{\rho}_{12}^2/\hat{\rho}_{22}}{\mu}\right)^{1/2} \tag{15}$$

where only one solution is a relevant incoming wave ($\mathrm{Re}(k_S)>0$).

2.2 Rayleigh waves on a permeable free-surface

The Rayleigh waves are surface waves that exist when a half-space is in contact with the vacuum through its free-surface. For a half-space $y \leq 0$, three different cases can be considered at the free-surface $y = 0$: permeable ($\tau_{ij} n_j = 0$, $\tau = 0$), impermeable ($(\tau_{ij} + \tau\delta_{ij}) n_j = 0$, $(U_j - u_j) n_j = 0$) or partially permeable. In this paper, only the permeable case is considered.

The potentials for the surface mode are composed by unknown functions $R_i = R_i(y)$ and a wave propagating in the positive x direction:

$$\varphi_i = R_i^{(\mathrm{P})} e^{-ik_{\mathrm{R}}x}, \quad \psi_i = R_i^{(\mathrm{S})} e^{-ik_{\mathrm{R}}x} \tag{16}$$

Once substituted into the governing equations, a set of four ordinary differential equations are obtained. It can be converted into a fourth order equation in terms of $R_1^{(\mathrm{P})}$, and a second order equation in terms of $R_1^{(\mathrm{S})}$. The solution of the fourth order equation leads to:

$$R_1^{(\mathrm{P})} = P_{11} e^{k_{\mathrm{RP1}} y} + P_{12} e^{k_{\mathrm{RP2}} y} \tag{17}$$

$$\begin{aligned} R_2^{(\mathrm{P})} &= P_{21} e^{k_{\mathrm{RP1}} y} + P_{22} e^{k_{\mathrm{RP2}} y} = D_1 P_{11} e^{k_{\mathrm{RP1}} y} + D_2 P_{12} e^{k_{\mathrm{RP2}} y} \\ D_j &= \frac{(\lambda + 2\mu) k_{Pj}^2 - \omega^2 (\hat{\rho}_{11} - Q/R\hat{\rho}_{12})}{\omega^2 (\hat{\rho}_{12} - Q/R\hat{\rho}_{22})} \end{aligned} \tag{18}$$

where the wavenumbers $k_{\mathrm{RP}j}$ are obtained from:

$$k_{\mathrm{RPj}} = \pm\sqrt{k_{\mathrm{R}}^2 - k_{\mathrm{Pj}}^2} \tag{19}$$

being physically meaningful only those with $\mathrm{Re}(k_{\mathrm{RP}j}) > 0$, i.e. those producing evanescent displacements when $y \to -\infty$. The solution of the second order equation leads to:

$$R_1^{(\mathrm{S})} = S_1 e^{k_{\mathrm{RS}} y} \tag{20}$$

$$R_2^{(\mathrm{S})} = S_2 e^{k_{\mathrm{RS}} y} = -\hat{\rho}_{12}/\hat{\rho}_{22} e^{k_{\mathrm{RS}} y} \tag{21}$$

where the wavenumber k_{S} is:

$$k_{\mathrm{RS}} = \pm\sqrt{k_{\mathrm{R}}^2 - k_S^2} \tag{22}$$

being meaningful only that with $\mathrm{Re}(k_{\mathrm{RS}}) > 0$. Therefore, the potentials are:

$$\varphi_i = \left(P_{i1} e^{k_{\mathrm{RP1}} y} + P_{i2} e^{k_{\mathrm{RP2}} y} \right) e^{-ik_{\mathrm{R}}x}, \quad \psi_i = S_i e^{k_{\mathrm{RS}} y} e^{-ik_{\mathrm{R}}x} \tag{23}$$

At this point, displacements and stresses can be written as functions of three amplitudes (P_{11}, P_{12} and S_1) and the Rayleigh wavenumber k_{R}. Applying the permeable boundary conditions $\tau_{xy} = 0$, $\tau_{yy} = 0$ and $\tau = 0$ to the free-surface at $y = 0$, one obtains the following set of three equations:

$$\begin{aligned} \left[-2\mu i k_{\mathrm{R}} k_{\mathrm{RP1}} \right] P_{11} + \left[-2\mu i k_{\mathrm{R}} k_{\mathrm{RP2}} \right] P_{12} + \left[\mu \left(2k_{\mathrm{R}}^2 - k_{\mathrm{S}}^2 \right) \right] S_1 &= 0 \\ \left[2\mu k_{\mathrm{R}}^2 - (N + QD_1) k_{\mathrm{P1}}^2 \right] P_{11} + \left[2\mu k_{\mathrm{R}}^2 - (N + QD_2) k_{\mathrm{P2}}^2 \right] P_{12} + \left[2\mu i k_{\mathrm{R}} k_{\mathrm{RS}} \right] S_1 &= 0 \\ \left[-(Q + RD_1) k_{\mathrm{P1}}^2 \right] P_{11} + \left[-(Q + RD_2) k_{\mathrm{P2}}^2 \right] P_{12} &= 0 \end{aligned} \tag{24}$$

where $N = \lambda + 2\mu + Q^2/R$. After some algebraic manipulations using the relationships between wavenumbers given by Eqs. (12), (15), (19) and (22), the characteristic equation associated with this homogeneous set of equations can be written in a similar fashion than that of the elastic case [1, Eq. (5.95)]:

$$\left(2 - r^2\right)^2 - 4\sqrt{1 - r^2} \left(H_2 \sqrt{1 - G_1 r^2} - H_1 \sqrt{1 - G_2 r^2} \right) = 0 \tag{25}$$

where:

$$r = \frac{k_{\mathrm{S}}}{k_{\mathrm{R}}}, \quad H_j = \frac{[\mu/(\lambda + 2\mu)] k_{\mathrm{S}}^2 - k_{\mathrm{P}j}^2}{k_{\mathrm{P1}}^2 - k_{\mathrm{P2}}^2}, \quad G_j = \frac{k_{\mathrm{P}j}^2}{k_S^2} \tag{26}$$

Eq. (25) is arranged in a new way which is more tractable than others previously obtained, e.g. [16, 36]. In fact, all terms are dimensionless, well behaved, and depend only on the bulk wavenumbers and Lamé's parameters. It is direct to verify that this equation collapse into the elastic equation; if $\phi \to 0$, then $k_{\mathrm{P1}} \to 0$, $k_{\mathrm{P2}} \to k_{\mathrm{P}}^{\mathrm{elastic}}$, $k_S \to k_{\mathrm{S}}^{\mathrm{elastic}}$ and $(\lambda + 2\mu)/\mu \to (k_{\mathrm{S}}^{\mathrm{elastic}}/k_{\mathrm{P}}^{\mathrm{elastic}})^2$.

2.3 Conventional and Dual Boundary Element Method

The poroelastic soil region is treated numerically using the BEM. Two classes of region boundaries are considered: ordinary and crack-like. A crack-like boundary is an oriented boundary composed by two boundaries sharing the same space but with opposite orientations. It represents the idealization of a null thickness discontinuity within the region: a crack (void) or an inclusion. The BEM relies on the discretization of the Boundary Integral Equations (BIE) used to build a solvable linear system of equations. The conventional BEM uses the Singular BIE (SBIE), and it is able to deal with ordinary boundaries but not with crack-like boundaries. This occurs because identical SBIE are obtained when collocating them on the crack-like boundary, leading to a singular linear system of equations. It can be solved by using the Dual BEM [23, 31] (DBEM) when collocating on a crack-like boundary. The DBEM is a proper combination of the SBIE and the Hypersingular BIE (HBIE), which is commonly used for crack analysis. However, in this work, it is used to couple a crack-like boundary with an elastic inclusion modeled as a structural member.

Cheng et al. [**?**] and Domínguez [**?**, 17] presented almost simultaneously an equivalent formulation of the Biot's poroelasticity. However, Domínguez's weighted residual formulation is particularly handy as it has a clear connection to the well-known acoustic and elastodynamic formulations. To the authors' knowledge, only the SBIE has been treated so far, thus the HBIE and the DBIE are presented here with some detail.

Let Ω be a Biot poroelastic region, and $\Gamma = \partial\Gamma$ its boundary with outward unit normal $\mathbf{n}$. The SBIE for a collocation point $\mathbf{x}^i$ not located at a crack-like boundary can be written as [**?**, 17]:

$$\begin{gathered}\begin{bmatrix} Jc^i_{00} & 0 \\ 0 & c^i_{lk} \end{bmatrix} \begin{Bmatrix} \tau^i \\ u^i_k \end{Bmatrix} + \int_\Gamma \begin{bmatrix} -(U^*_{n00} + JX'^*_j n_j)\, t^*_{0k} \\ -U^*_{nl0} \qquad\quad t^*_{lk} \end{bmatrix} \begin{Bmatrix} \tau \\ u_k \end{Bmatrix} \mathrm{d}\Gamma = \int_\Gamma \begin{bmatrix} -\tau^*_{00} & u^*_{0k} \\ -\tau^*_{l0} & u^*_{lk} \end{bmatrix} \begin{Bmatrix} U_n \\ t_k \end{Bmatrix} \mathrm{d}\Gamma \\ \mathbf{C}^i\mathbf{u}^i + \int_\Gamma \mathbf{T}^*\mathbf{u}\,\mathrm{d}\Gamma = \int_\Gamma \mathbf{U}^*\mathbf{t}\,\mathrm{d}\Gamma \end{gathered} \tag{27}$$

where indicial notation $l,k \in [1,2]$ with summation convention is used, and body forces has been neglected. The secondary variables at the boundary are the fluid normal displacement $U_n = U_k n_k$ and the solid traction $t_l = \tau_{lk} n_k$. The vector $\mathbf{u}$ contains all the primary variables, while $\mathbf{t}$ contains all the secondary variables. The fundamental solution matrix $\mathbf{U}^*$ was obtained by Dominguez [17] using the Kupradze procedure [25], and was written in a compact form. However, in order to ease the developments done in the present work, we follow the idea of Maeso et al. [28] of writing the fundamental solution separately in a way that resembles the fundamental solutions of acoustics and elastodynamics:

$$\tau^*_{00} = \frac{1}{2\pi}\eta, \quad \eta = \frac{1}{k_1^2 - k_2^2}\left[\alpha_1 \mathrm{K}_0(ik_1 r) - \alpha_2 \mathrm{K}_0(ik_2 r)\right], \quad \alpha_j = k_j^2 - \frac{\mu}{\lambda + 2\mu}k_3^2 \tag{28}$$

$$u^*_{0k} = -\frac{1}{2\pi}\Theta r_{,k}, \quad \Theta = \left(\frac{Q}{R} - Z\right)\frac{1}{\lambda + 2\mu}\frac{1}{k_1^2 - k_2^2}\left[ik_1 \mathrm{K}_1(ik_1 r) - ik_2 \mathrm{K}_1(ik_2 r)\right] \tag{29}$$

$$\tau^*_{l0} = \frac{1}{2\pi J}\Theta r_{,l} \tag{30}$$

$$\begin{aligned} u^*_{lk} &= \frac{1}{2\pi\mu}\left(\psi\delta_{lk} - \chi r_{,l} r_{,k}\right) \\ \psi &= \mathrm{K}_0(ik_3 r) + \frac{1}{ik_3 r}\mathrm{K}_1(ik_3 r) - \frac{1}{k_1^2 - k_2^2}\left[\beta_1 \frac{1}{ik_1 r}\mathrm{K}_1(ik_1 r) - \beta_2 \frac{1}{ik_2 r}\mathrm{K}_1(ik_2 r)\right] \\ \chi &= \mathrm{K}_2(ik_3 r) - \frac{1}{k_1^2 - k_2^2}\left[\beta_1 \mathrm{K}_2(ik_1 r) - \beta_2 \mathrm{K}_2(ik_2 r)\right], \quad \beta_j = \frac{\mu}{\lambda + 2\mu}k_j^2 - \frac{k_1^2 k_2^2}{k_3^2} \end{aligned} \tag{31}$$

where $r = |\mathbf{x} - \mathbf{x}^i|$ is the distance between collocation and observation points, $k_1 = k_{\mathrm{P1}}$, $k_2 = k_{\mathrm{P2}}$, $k_3 = k_{\mathrm{S}}$, $J = 1/(\hat{\rho}_{22}\omega^2)$, $Z = \hat{\rho}_{12}/\hat{\rho}_{22}$, and $\mathrm{K}_n(z)$ is the modified Bessel function of the second kind, order n and argument z. By doing so, the fundamental solution matrix $\mathbf{U}^*$ is composed by four submatrices: *00*, *0k*, *l0* and *lk*; where the first index is associated with the load and the second index with the observation, being *0* associated with the fluid phase and l,k with the solid phase. Also, the diagonal submatrices *00* and *lk* have the same kind of singularities as the well known acoustics and elastodynamic problems, respectively. In fact, the free-terms c^i_{00} and c^i_{lk} are completely similar to that problems. The off-diagonal submatrices *0k* and *l0* associated with the coupling between phases have one lower order of singularity than the diagonal submatrices. Using Eqs. (2), (3) and (4), the fundamental solution matrix $\mathbf{T}^*$ can be obtained from:

$$U^*_{n00} + JX'^*_j n_j = -J\tau^*_{00,j} n_j - Zu^*_{0j} n_j \tag{32}$$

$$t^*_{0k} = \left[\lambda u^*_{0m,m}\delta_{kj} + \mu\left(u^*_{0k,j} + u^*_{0j,k}\right)\right] n_j + \frac{Q}{R}\tau^*_{00} n_k \tag{33}$$

$$U^*_{nl0} = -J\tau^*_{l0,j} n_j - Zu^*_{lj} n_j \tag{34}$$

$$t^*_{lk} = \left[\lambda u^*_{lm,m}\delta_{kj} + \mu\left(u^*_{lk,j} + u^*_{lj,k}\right)\right] n_j + \frac{Q}{R}\tau^*_{l0} n_k \tag{35}$$

which again can be written in a way that resembles the corresponding fundamental solutions of acoustics and elastodynamics, see A. The HBIE is obtained by establishing the secondary variables at the collocation point, which requires the SBIE and its derivatives with respect to the coordinates of the collocation point:

$$U^i_n = U^i_j n^i_j = -J\tau^i_{,j} n^i_j - Zu^i_j n^i_j \tag{36}$$

$$t^i_l = \tau^i_{lj} n^i_j = \left[\lambda u^i_{m,m}\delta_{lj} + \mu\left(u^i_{l,j} + u^i_{j,l}\right)\right] n^i_j + \frac{Q}{R}\tau^i n^i_l \tag{37}$$

where $\mathbf{n}^i$ is the unit normal at the collocation point, and the comma notation denotes $\partial/\partial x_k^i$ instead of the usual $\partial/\partial x_k$ that is used in the rest of the paper. When considering a collocation point located at a boundary, corner points are excluded in order to avoid multivalued $\mathbf{n}^i$, thus $\Gamma(\mathbf{x}^i) \in \mathscr{C}^1$ holds for the HBIE. Therefore, the HBIE can be written as:

$$\begin{aligned} c^i \begin{bmatrix} 1 & 0 \\ 0 & \delta_{lk} \end{bmatrix} \begin{Bmatrix} U_n^i \\ t_k^i \end{Bmatrix} + \int_\Gamma \begin{bmatrix} -s_{00}^* & s_{0k}^* \\ -s_{l0}^* & s_{lk}^* \end{bmatrix} \begin{Bmatrix} \tau \\ u_k \end{Bmatrix} \mathrm{d}\Gamma = \int_\Gamma \begin{bmatrix} -d_{00}^* & d_{0k}^* \\ -d_{l0}^* & d_{lk}^* \end{bmatrix} \begin{Bmatrix} U_n \\ t_k \end{Bmatrix} \mathrm{d}\Gamma \\ \mathbf{C}^i \mathbf{t}^i + \int_\Gamma \mathbf{S}^* \mathbf{u} \, \mathrm{d}\Gamma = \int_\Gamma \mathbf{D}^* \mathbf{t} \, \mathrm{d}\Gamma \end{aligned} \tag{38}$$

where again the diagonal submatrices of $\mathbf{D}^*$ and $\mathbf{S}^*$ and the free-term resemble those of acoustics and elastodynamic problems. The matrices $\mathbf{D}^*$ and $\mathbf{S}^*$ are written in A. When $\mathbf{x}^i \in \Gamma$, both the SBIE and the HBIE contain singular integrals, being at most weakly singular those associated with $\mathbf{U}^*$, at most strongly singular (Cauchy Principal Value integrals) those associated with $\mathbf{T}^*$ and $\mathbf{D}^*$, and at most hypersingular (Hadamard Finite Part integrals) those associated with $\mathbf{S}^*$. The treatment of those integrals for this problem is analogous to that of acoustics [10] and elastodynamics [32, 14] problems. The treatment of the HBIE is based on a regularization process that requires the integrands (excluding the term r^{-2}) belong to the Hölder function space $\mathscr{C}^{1,\alpha}$ [29]. To do so, the collocation point must be in a boundary point where the primary variables are continuous, i.e. $\mathbf{u}^i \in \mathscr{C}^1$.

The SBIE and HBIE shown in Eqs. (27) and (38), respectively, are valid for a collocation point located inside or outside the domain, and at an ordinary boundary, with the condition that $\Gamma(\mathbf{x}^i) \in \mathscr{C}^1$ and $\mathbf{u}^i \in \mathscr{C}^1$ for the HBIE. However, for a collocation point located at a crack-like boundary, the BIEs have to be modified. A crack-like boundary is composed by two sub-boundaries, denoted as positive $+$ and negative $-$ faces. Hence, the integration domain associated with a crack-like boundary can be divided into these two faces, which are geometrically coincident but have opposite orientations. Taking into account this, the BIEs for a collocation point located at a crack-like boundary can be built using a limit to the boundary approach, see e.g. [10]. In this case, the SBIE and HBIE can be written as:

$$\frac{1}{2} \begin{bmatrix} J & 0 \\ 0 & \delta_{lk} \end{bmatrix} \left(\mathbf{u}^{i+} + \mathbf{u}^{i-} \right) + \int_\Gamma \mathbf{T}^* \mathbf{u} \, \mathrm{d}\Gamma = \int_\Gamma \mathbf{U}^* \mathbf{t} \, \mathrm{d}\Gamma \tag{39}$$

$$\frac{1}{2} \begin{bmatrix} 1 & 0 \\ 0 & \delta_{lk} \end{bmatrix} \left(\mathbf{t}^{i+} - \mathbf{t}^{i-} \right) + \int_\Gamma \mathbf{S}^* \mathbf{u} \, \mathrm{d}\Gamma = \int_\Gamma \mathbf{D}^* \mathbf{t} \, \mathrm{d}\Gamma \tag{40}$$

where it has been assumed that $\Gamma(\mathbf{x}^i) \in \mathscr{C}^1$ for both equations. Since each face has its own set of variables, $(\mathbf{u}^{i+}, \mathbf{t}^{i+})$ for the positive face and $(\mathbf{u}^{i-}, \mathbf{t}^{i-})$ for the negative face, and its own boundary conditions, two linearly independent BIEs are needed. By examining Eqs. (39) and (40), it is clear that neither the SBIE nor the HBIE are able to give independently enough conditions. Using both BIEs is the only way to directly get linearly independent equations for a crack-like boundary. Consequently, Eqs. (39) and (40) are called Dual BIEs [23], and their application to the BEM is called the Dual BEM [31].

In this work, the discretization of the BIEs is performed using quadratic elements. For ordinary boundaries, the SBIE is used in the conventional way using nodal collocation for all nodes, except at corner points where double nodes with non-nodal collocation are applied. For crack-like boundaries, the Dual BIEs are used applying the Multiple Collocation Approach [10, 21]. The Rayleigh incident field defined in Section 2.2 is introduced into the model by formulating the BIEs in terms of the scattered field [18].

2.4 Soil-structure coupling

The conventional BEM and the Dual BEM used to treat the poroelastic soil region, together with the structural FEM model of thin structures, and the appropriate coupling conditions, make possible building a general BEM-FEM model of soils interacting with plate-like structures. In this two-dimensional approach, thin structures of infinite depth are assumed, hence an equivalent two-dimensional beam model with a modified Young's modulus $E_\mathrm{m}/(1-\nu^2)$ can be used.

The beam finite element has been already described [10, 30], but a brief summary is given here for the sake of completeness. Let's consider an elastic material with Young's modulus E_m, Poisson's ratio ν, and hysteretic damping coefficient ξ. Then, the effective beam Young's modulus including the hysteretic damping is $E = E_\mathrm{m}(1+i2\xi)/(1-\nu^2)$. The beam is straight, with a cross-section defined by its area A and its inertia I, and follows the Euler-Bernoulli beam theory with added rotational inertia. It has three nodes and eight degrees of freedom: vertex nodes $i = 1, 2$ have translation $u_1^{(i)}, u_2^{(i)}$ and rotation $\theta^{(i)}$, while the central node $i = 3$ has only translation $u_1^{(3)}, u_2^{(3)}$. Axial and lateral quadratic distributed loads over each element are considered, being their nodal values $s_1'^{(i)}$ and $s_2'^{(i)}$, respectively. By doing so, a node-by-node correspondence between the beam finite element and the quadratic boundary element is achieved. Therefore, the element-wise FEM equation is:

$$\left(\mathbf{K} - \omega^2 \mathbf{M} \right) \cdot \mathbf{u} = \mathbf{Q} \cdot \mathbf{s}' \tag{41}$$

where $\mathbf{u}$ is the vector of kinematic variables in global coordinates, $\mathbf{s}'$ is the vector of distributed loads in local coordinates, $\mathbf{K}$ and $\mathbf{M}$ are the stiffness and mass matrices in global coordinates, respectively, and $\mathbf{Q}$ is the load matrix that converts distributed loads in local coordinates into equivalent nodal forces and moments in global coordinates.

The beam finite element can be coupled with an ordinary boundary element (BEM-FEM coupling) or with a crack-like boundary element (DBEM-FEM coupling), see Fig. 1. Let Υ_j^s be a beam finite element belonging to a elastic region Ω_s, and $\mathbf{x}_1', \mathbf{x}_2'$ its local axis. Let Γ be a boundary (ordinary or crack-like) of a poroelastic region Ω_p, being the orientation of Γ defined by its outward unit normal vector $\mathbf{n}$, and Υ_j a boundary element of that boundary. Assuming an impermeable interface with perfect bonding between Γ and $\partial\Omega_\mathrm{s}$, the coupling conditions when Γ is an ordinary boundary consist of the following compatibility and equilibrium equations:

$$U_n^{(i)} = u_k^{(i)} n_k \tag{42}$$

$$u_l^{(i)} = u_l^{(\mathrm{is})} \tag{43}$$

$$\tau^{(i)} n_l + t_l^{(i)} + s_1'^{(\mathrm{is})} x_{1l}' + s_2'^{(\mathrm{is})} x_{2l}' = 0 \tag{44}$$

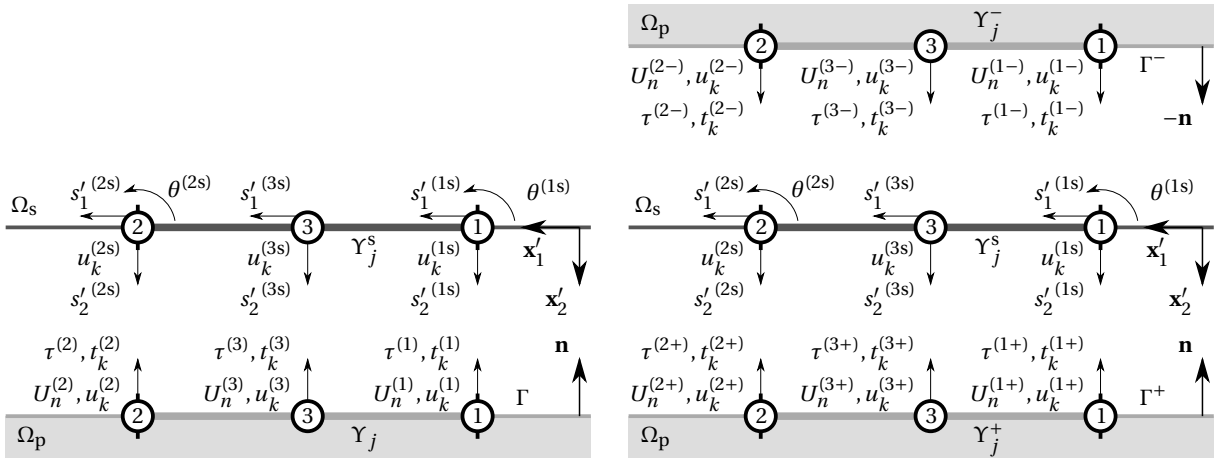

Figure 1: Types of coupling. Left: poroelastic ordinary boundary element - beam finite element (BEM-FEM coupling). Right: poroelastic crack-like boundary element - beam finite element (DBEM-FEM coupling).

where indicial notation $l,k \in [1,2]$ with summation convention is used, and i is the local index of a node. The coupling conditions when Γ is a crack-like boundary consist of the following compatibility and equilibrium equations:

$$U_n^{(i+)} = u_k^{(i+)} n_k \tag{45}$$

$$U_n^{(i-)} = -u_k^{(i-)} n_k \tag{46}$$

$$u_l^{(i+)} = u_l^{(is)} \tag{47}$$

$$u_l^{(i-)} = u_l^{(is)} \tag{48}$$

$$\tau^{(i+)} n_l + t_l^{(i+)} - \tau^{(i-)} n_l + t_l^{(i-)} + s_1'^{(is)} x_{1l}' + s_2'^{(is)} x_{2l}' = 0 \tag{49}$$

If, instead of a poroelastic soil, an elastic soil or an inviscid fluid is considered, these coupling equations lead directly to the appropriate ones by simply removing the equations and variables that do not exist in that kind of medium.

3 Results and discussion

3.1 Comparison with published results

To the authors' knowledge, there are not any published results where directly validate the proposed numerical approach. However, is possible to compare it with published results obtained by other models sharing some aspects. Thereby, in this section it is compared with the classical vibration isolation paper by Beskos et al. [8].

Beskos et al. [8] studied the vibration isolation of open and filled trenches using a two-dimensional conventional BEM elastodynamic model. The problem under consideration is a trench, open or filled with concrete, with a depth to width ratio $d/w = 10$, impinged by waves coming from a footing $5d$ behind the trench, vibrating with a frequency corresponding to a Rayleigh wavelength λ_R equal to the depth d. The elastic soil has a density $\rho = 1785$ kg/m^3, shear modulus $\mu = 132$ MPa, Poisson's ratio $\nu = 0.25$ and hysteretic damping $\xi = 0.03$. The equivalent poroelastic soil used in our model has a porosity $\phi = 0.001$, fluid density $\rho_\mathrm{f} = 0.001$ kg/m^3, solid density $\rho_\mathrm{s} = 1785$ kg/m^3, null additional apparent density, solid Lamé's parameters $\mu = \lambda = 132$ MPa, solid phase hysteretic damping $\xi_\mathrm{s} = 0.03$, Biot's parameters $R = Q = 0.1$ MPa, and null dissipation coefficient. The concrete for the filled trench barrier has a density $\rho = 2449$ kg/m3, shear modulus $\mu = 4.52628$ GPa, Poisson's ratio $\nu = 0.25$ and hysteretic damping $\xi = 0.15$. Fig. 2 shows a comparison between their results and our results using the vertical displacement amplitude reduction ratio A_y:

$$A_y(x) = \frac{\left|u_y(x, y=0)\right|}{\left|u_y^{\text{no barrier}}(x, y=0)\right|} \tag{50}$$

For the open trench, we have used an open trench with $d/w = 10$ using a conventional BEM model, but also an open trench with the null width assumption ($d/w \to \infty$) using the Dual BEM. For the filled trench, we have used a filled trench with $d/w = 10$ using a conventional multidomain BEM model, and also a filled trench using our DBEM-FEM model, i.e. from the soil point of view the trench has null thickness but preserves its structural behaviour. There exist differences between the results of Beskos et al. and our results, although the main tendencies are similar. It is probably due to the fact that they used constant boundary elements and an important truncation of the free-surface mesh, which was also noticed by Ahmad et al. [2]. In both problems, the differences between the results using the real geometry (conventional BEM) and the results using the null width assumption (DBEM) are very small. Therefore, it is justified using the proposed DBEM-FEM model for thin structures ($d/w \geq 10$) in these kinds of problems.

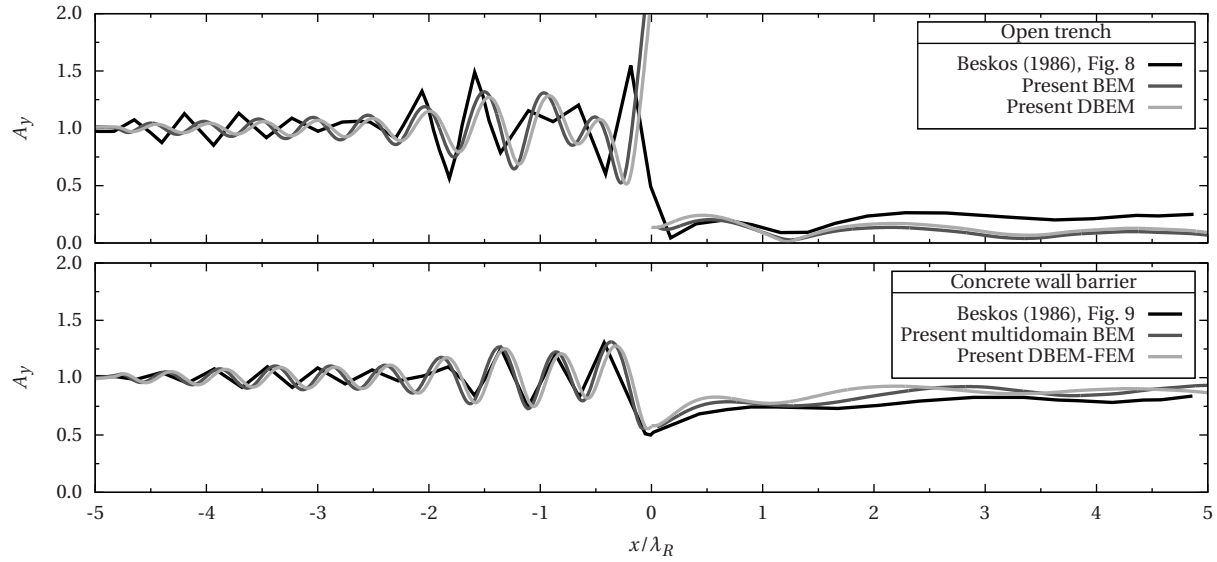

Figure 2: Comparison with Beskos et al. [8]

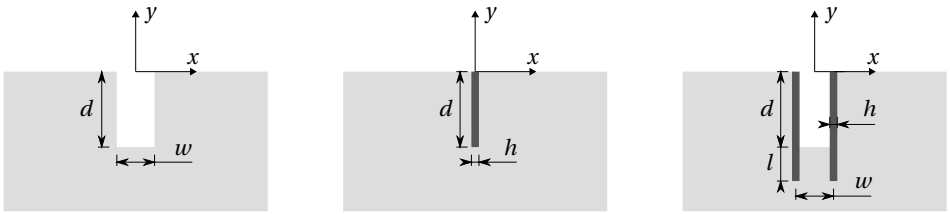

Figure 3: Problems layout. Left: open trench. Center: simple wall. Right: open trench-wall.

3.2 Wave barriers in poroelastic soils

Three kinds of wave barrier systems are studied: open trench, simple wall and open trench-wall; see Fig. 3. An open trench system is defined by its depth d and width w. Qualitatively, it acts as a perfect reflector where surface waves having a wavelength less than its depth are filtered out. A pure open trench is the perfect solution, however, systems using walls are needed in situations where the soil stability is compromised. In this study, we consider a wall characterized by its top view cross-section per unit length, see Fig. 4. It is defined by the total width h and the wall thickness t, being $t \leq h$. Hence, the cross-section area is $A = t$ and the inertia is $I = t^3/12 + t(h/2 - t/2)^2$. When $t = h$, it represents exactly a plate with uniform cross-section. When $t < h$, it represents a two-dimensional simplified version of a sheet pile, whose three-dimensional geometry and structural behaviour as a transversely isotropic plate are neglected. This simplification is valid as long as we are interested in far-field variables. A simple wall barrier system is defined by its depth d and wall cross-section. An open trench-wall system is defined by its trench depth d, trench width w, wall cross-section, and wall burial depth l. Hence, these problems are defined by their geometry: d, w, l, h and t; by the properties of their regions: poroelastic soil (ϕ, ρ_f, ρ_s, μ_s, λ_s, ξ_s, Q, R, ρ_a, b) and wall (ρ_b, E_b, ν_b, ξ_b); and by the frequency ω.

For elastic soils, the open trench and the simple wall problems have been extensively studied, whereas the open trench-wall system has been rarely studied [33]. In these cases, each problem is easily nondimensionalized to a small set of parameters of general applicability. Basically, ratios of lengths (d/w, d/h, etc.), Poisson's ratios of the soil ν_s and wall ν_b, ratios of densities $\rho_\mathrm{s}/\rho_\mathrm{b}$ and Young's modulus $E_\mathrm{s}/E_\mathrm{b}$ between soil and wall, and a dimensionless frequency ω^* defined by using the Rayleigh wave speed and some length, for example d. However, such a broad study for poroelastic soils is difficult due to the number of properties involved, and the question if a set of values for these properties represents an existing soil or not.

Therefore, in order to obtain realistic results of practical usage, we limit our study to water-saturated sandstones whose properties are based on experimental data. The poroelastic approximation of water-saturated sandstones is taken from [27], although a more general dissipative soil ($b \neq 0$)

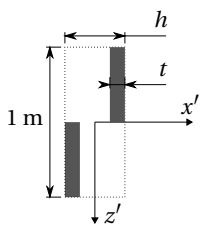

Figure 4: Wall cross-section

is considered here. The main hypothesis is the linear relationship between porosity ϕ and solid dry bulk modulus K_s:

$$K_s = K_{cr} + \left(1 - \frac{\phi}{\phi_{cr}}\right)\left(K_g - K_{cr}\right) \tag{51}$$

where $K_{cr} = 200\,\text{MPa}$ is the critical bulk modulus for the dry frame, $\phi_{cr} = 0.36$ is the critical porosity and $K_g = 36000\,\text{MPa}$ is the bulk modulus of a solid grain. The critical porosity ϕ_{cr} is the point where the porosity is too large to form a sustainable dry frame. Several porosities and Poisson's ratios are considered: $\phi = \{0.10, 0.20, 0.30\}$ and $\nu_s = \{0.20, 0.30, 0.40\}$. Thus, Lamé parameters are $\lambda_s = (3\nu_s)/(1+\nu_s)K_s$ and $\mu_s = [3(1-2\nu_s)]/[2(1+\nu_s)]K_s$. The density of the solid phase is $\rho_s = 2650\,\text{kg/m}^3$, and the damping ratio is null ($\xi_s = 0$). The fluid phase (water) properties are $K_f = 2000\,\text{MPa}$ and $\rho_f = 1000\,\text{kg/m}^3$. The Biot's coupling parameters Q and R are:

$$Q = \phi\frac{1-\phi-K_s/K_g}{(1-\phi-K_s/K_g)+\phi K_g/K_f}K_g, \quad R = \frac{\phi^2}{(1-\phi-K_s/K_g)+\phi K_g/K_f}K_g \tag{52}$$

Berryman's model for the additional aparent density [7] is used assuming spherical grains: $\rho_a = (1-\phi)\rho_f/2$. The dissipation coefficient is $b = \rho_f g\phi^2/\kappa$, where κ is the hydraulic conductivity. In order to present a dimensionless problem, a dimensionless dissipation coefficient $b^* = bd/\sqrt{\mu_s\rho}$ is defined, where $\rho = \phi\rho_f + (1-\phi)\rho_s$ is the bulk density. Also, it is necessary to use a dimensionless frequency ω^*. One representing the ratio between the barrier system depth and the Rayleigh wavelength $\omega^* = d/\lambda_{R0} = (\omega d)/(2\pi c_{R0})$ is defined, where c_{R0} is the wave speed of the Rayleigh waves assuming $b = 0$. Assuming a typical barrier depth $d \sim 5$ m, and taking into account that $\kappa \in [10^{-6}, 10^{-2}]$ m/s (see [27, Fig. 1]), $\phi \in [0.10, 0.30]$ and $\nu \in [0.20, 0.40]$, an appropriate set of values for the dimensionless dissipation coefficient is $b^* = \{0, 0.2, 5, 100, 2000\}$. For the dimensionless frequency, a suitable range $\omega^* \in [0.5, 1.5]$ is used. The thin walls are considered made of steel: $\rho_b = 7850\,\text{kg/m}^3$, $E_b = 210\,\text{GPa}$, $\nu_b = 0.30$, $\xi_b = 0.05$.

All the boundaries in contact with air are considered permeable, and given that the bulk modulus of the air is much more lower than any of the porous media, the fluid dynamic stress τ and the solid stresses τ_{ij} can be considered null at those boundaries. Specifically, these boundaries are the free-surface of the half-space and the bottom of the open trench-wall.

The isolation efficiency of each configuration is measured by using the average vertical displacement amplitude reduction ratio $\bar{A}_y$:

$$\bar{A}_y = \frac{1}{10\lambda_{R0} - a/2}\int_{a/2}^{10\lambda_{R0}} A_y(x)\,\mathrm{d}x \tag{53}$$

where $a = w$ for the open trench and open trench-wall, and $a = 0$ for the simple barrier. It synthesizes the behaviour of $A_y(x)$ along the shadow zone of the wave barrier up to $10\lambda_{R0}$, as suggested by Ahmad et al. [2].

3.2.1 Open trench

Three geometrical configurations of the open trench are studied: $d/w = \{1, 2, 10\}$; which correspond to a very wide, wide and narrow open trenches, respectively. Although it does not use any of the new features proposed here, it is mandatory since, to the authors' knowledge, previous results about this problem does not exist in the literature.

Fig. 5 shows $\bar{A}_y$ response for the ranges of variation of porosity ϕ, Poisson's ratio ν_s, dimensionless dissipation coefficient b^*, and dimensionless frequency ω^*, for the wide trench ($d/w = 2$). The main behaviour of open trenches in poroelastic soils are similar to those in elastic soils. The dimensionless frequency $\omega^* = d/\lambda_R = 1$ is a key point. Below this frequency, the efficiency gets worse increasingly, and above it, the efficiency improves up to a maximum efficiency, approximately constant for $\omega^* > 1.2$. In most cases, the Poisson's ratio has a small influence on $\bar{A}_y$ when $\omega^* > 0.8$. It becomes more important when the porosity is near ϕ_{cr} and the dimensionless dissipation coefficient is $b^* < 1$. The dimensionless dissipation coefficient b^* has a very small influence on $\bar{A}_y$ for $b^* > 5$. For $b^* < 5$, b^* becomes more influential when the porosity approaches ϕ_{cr}.

Fig. 6 shows $\bar{A}_y$ responses for the different d/w ratios, when $\nu_s = 0.30$ and $b^* \leq 5$. In general terms, the smaller d/w ratio the more efficient is the open trench, which is physically obvious. The influence of d/w increases as ω^* decreases, especially when $\omega^* < 0.6$. When $\omega^* > 1.2$, although differences exist, they are less important given the high efficiency ($\bar{A}_y < 0.05$) of all the studied d/w ratios. The influence of the porosity ϕ and the dissipation coefficient b^* is similar for the different studied d/w ratios.

3.2.2 Simple barrier

The simple barrier is studied for three depth to cross-section width ratios: $d/h = \{10, 20, 100\}$; and each of them for four cross-section width to wall thickness ratios: $h/t = \{1, 6, 10, 20\}$. Except for the average efficiency level, which is much more lower, the influence of soil properties over the $\bar{A}_y$ response for simple barriers are similar to those of open trenches. Therefore, in order to compare the influence of the wall configuration, the soil properties are fixed to: $\phi = 0.20$, $b^* = 0.2$, $\nu_s = 0.30$. These problems are solved using the proposed DBEM-FEM coupling. Hence, the soil sees a null thickness barrier which maintains its effective structural response. Additionally, the real three-dimensional behaviour of cross-sections with $h/t \neq 1$ is approximated by a two-dimensional behaviour, which is a valid assumption as long as we are not concerned about near-field variables.

Fig. 7 shows $\bar{A}_y$ response for different d/h and h/t ratios. For the studied range of ω^*, the efficiency of the simple barrier is much more lower than the efficiency of any open trench. While the open trench acts as a perfect reflector, the simple barrier partially converts surface waves into body waves. As pointed out by Ahmad et al. [2], the efficiency of this type of barriers depends mostly on the wall area $d \cdot t$. In order to show this relationship for the present study, Fig. 8 has been built using the $\bar{A}_y$ analysis points of all cases shown in Fig. 7 in ordinates, and a dimensionless area $(d/\lambda_{R0})(t/\lambda_{R0}) = (\omega^*)^2(h/d)(t/h)$ in abscissas. The left graph shows a global picture of the results, and the right graph shows a detailed view of the results for smaller cross-sections. Although the observed slope is different for each specific cross-section, it is shown that, as found by Ahmad et al., a roughly linear relationship exists between the efficiency and the dimensionless area.

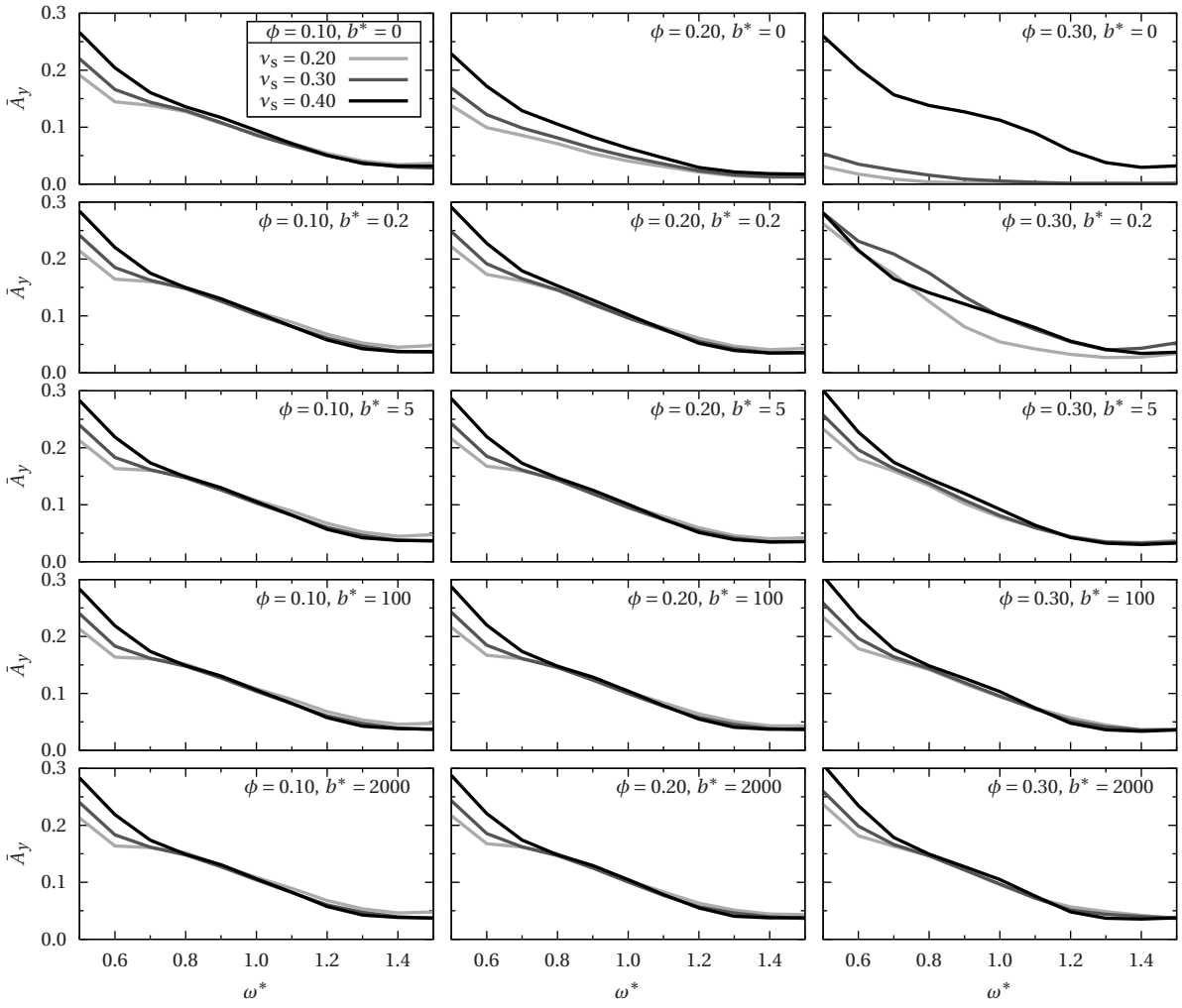

Figure 5: $\bar{A}_y$ response for open trench $d/w = 2$

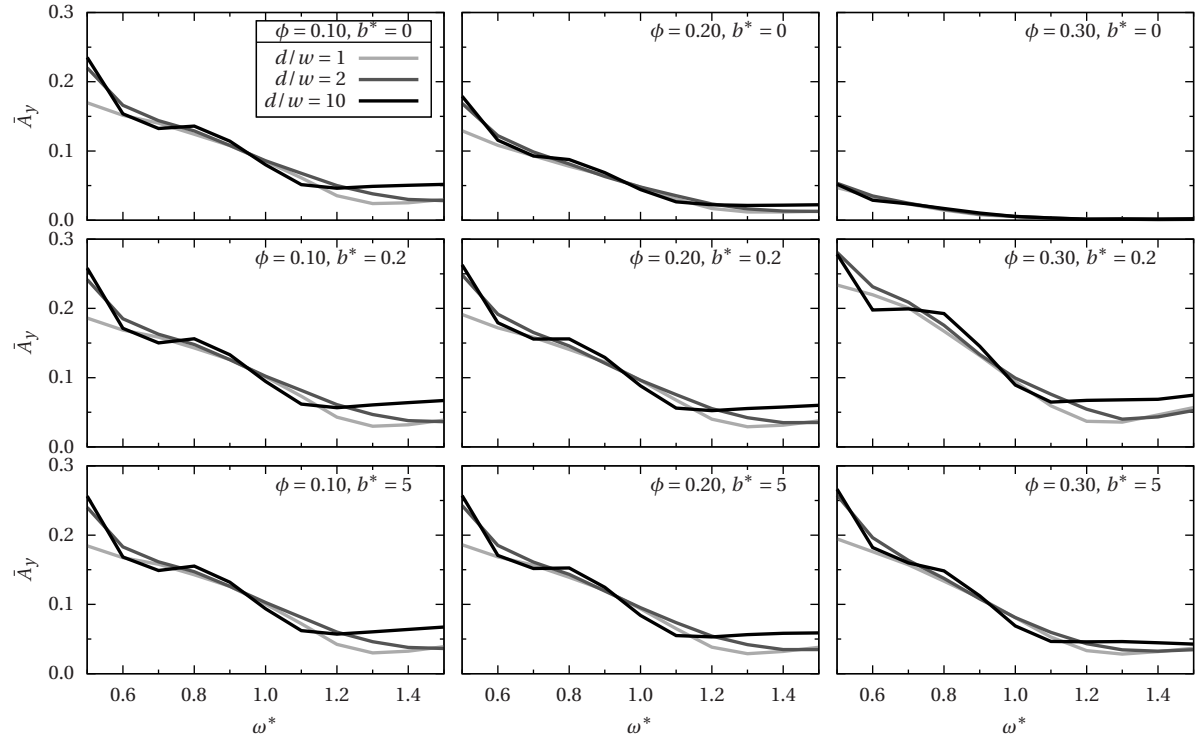

Figure 6: $\bar{A}_y$ comparison between open trenches with different d/w ratios ($\nu_s = 0.30$)

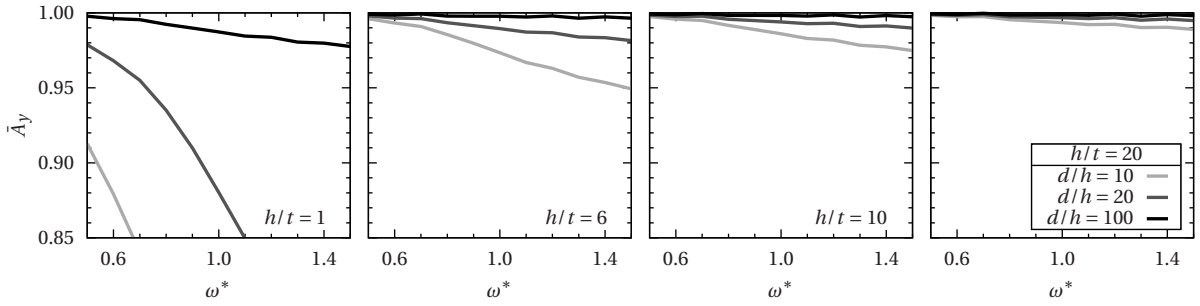

Figure 7: $\bar{A}_y$ comparison between simple barriers with different d/h and h/t ratios ($\phi = 0.20$, $b^* = 0.2$, $\nu_s = 0.30$)

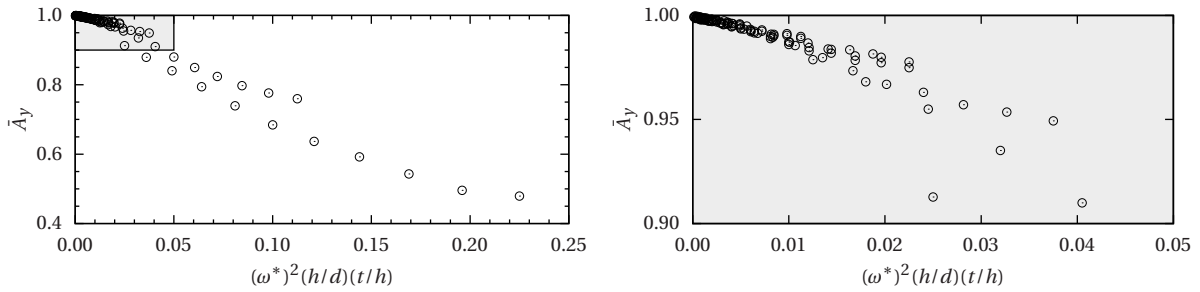

Figure 8: $\bar{A}_y$ comparison between simple barriers using the dimensionless area in abscissas ($\phi = 0.20$, $b^* = 0.2$, $\nu_s = 0.30$)

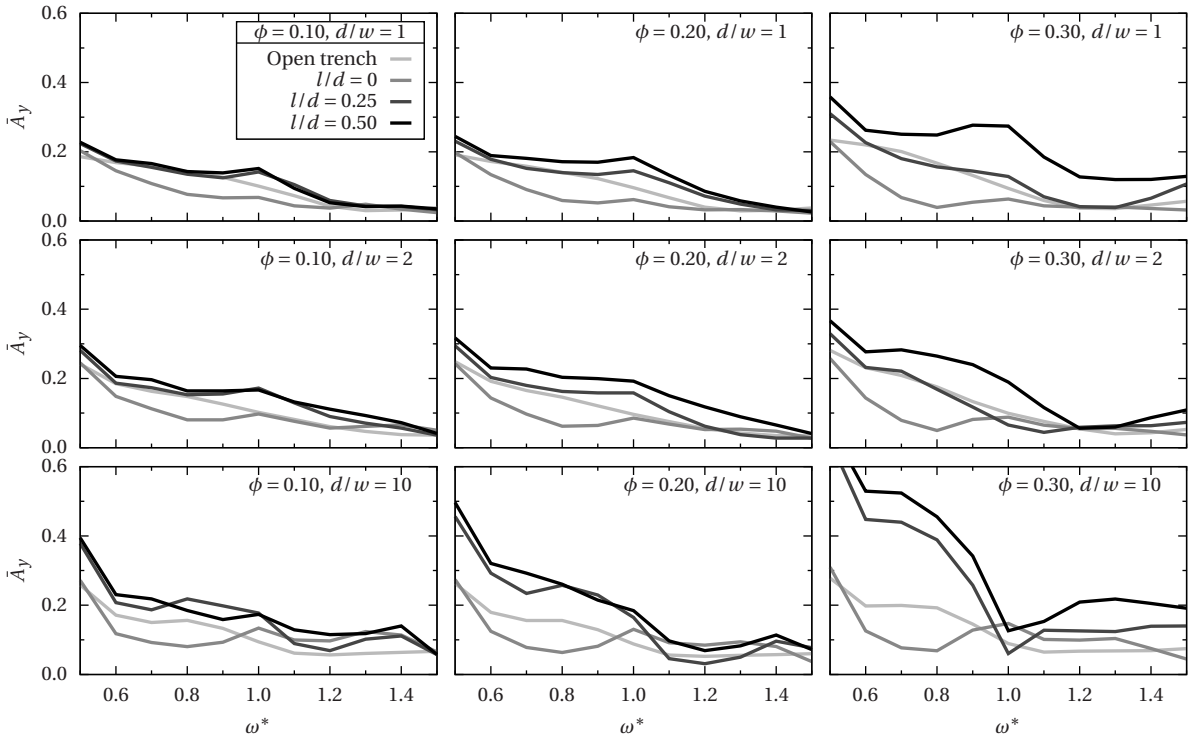

Figure 9: $\bar{A}_y$ comparison between open trench and open trench-wall for different ϕ, d/w and l/d ratios ($b^* = 0.2$, $\nu_s = 0.30$, $d/h = 20$, $h/t = 1$)

3.2.3 Open trench-wall

The open trench-wall is studied for three depth to width ratios: $d/w = \{1, 2, 10\}$; three wall burial depth to trench depth ratios: $l/d = \{0, 0.25, 0.50\}$; three trench depth to cross-section width ratios: $d/h = \{10, 20, 100\}$; and four cross-section width to wall thickness ratios: $h/t = \{1, 6, 10, 20\}$. The influence of the dimensionless dissipation coefficient b^* and the Poisson's ratio ν_s is similar to that of the open trenches, i.e. their influence is relatively small, thus $b^* = 0.2$ and $\nu_s = 0.30$ are assumed. These problems are solved using both the BEM-FEM and DBEM-FEM couplings, being the BEM-FEM coupling applied to the retaining part of walls, and the DBEM-FEM coupling applied to the buried part of the walls.

Fig. 9 has been built in order to assess the influence of the wall and its burying in the soil over $\bar{A}_y$. For all cases, the depth to cross-section width ratio is $d/h = 20$, and the cross-section width to wall thickness ratio is $h/t = 1$. The figure contains 3×3 graphs, where each column corresponds to a different porosity ϕ, and each row to a different depth to width d/w ratio. Each graph contains four curves corresponding to the open trench case and the open trench-wall case with three different wall burial depth to trench depth l/d ratios. For a given ϕ and d/w ratio, the differences between the open trench and the open trench-wall for $l/d = 0$ are small for $\omega^* > 1$, but for $\omega^* < 1$ the open trench-wall is slightly more efficient. For the other values of the l/d ratio, $\bar{A}_y$ gets worse, especially for $\omega^* < 1$. The smaller the porosity, the smaller $\bar{A}_y$ differences between the open trench and the open trench-wall for any l/d ratio. Likewise, the smaller the d/w ratio, the smaller the $\bar{A}_y$ differences between both kinds of wave barriers.

Fig. 10 contains graphs comparing the $\bar{A}_y$ response of configurations with different l/d ratios and different cross-sections. For all cases, the porosity is $\phi = 0.20$, and the depth to width ratio is $d/w = 2$. Each column corresponds to a different d/h ratio, and each row correspond to a different l/d ratio. Four curves are drawn on each graph, one corresponding with the open trench, and three corresponding with $h/t = \{1, 6, 20\}$. It is seen that the open trench-wall converges to the open trench as d/h and h/t increase, as it should be. The cross-sections corresponding with a plate with uniform thickness ($h/t = 1$) have a considerable impact on $\bar{A}_y$, increasing the efficiency for $\omega^* < 1$ and $l/d = 0$, but decreasing it in the rest of the cases. The cross-sections associated with the sheet pile idealization have a small influence on the efficiency when compared with the open trench.

4 Conclusions

It has been developed a two-dimensional time harmonic model combining the BEM and the FEM for the isolation efficiency analysis of total or partially buried thin walled wave barriers in poroelastic soils. The SBIE and the HBIE needed for the conventional BEM and the Dual BEM for poroelastic regions have been obtained. Also, we describe the coupling conditions between a beam finite element and an ordinary boundary (BEM-FEM), and between a beam finite element and a crack-like boundary (DBEM-FEM), being the latter a new type of coupling element. The considered ground vibrations are Rayleigh waves propagating on a permeable free-surface, which have been obtained, and whose characteristic equation is written is simple new form.

The open trench, simple wall and open trench-wall are studied varying their geometry, soil properties and frequency. The soil is assumed to be a sandstone following a linear relationship between porosity and solid dry bulk modulus. In the study, several values of porosity ϕ, Poisson's ratio ν_s and dimensionless dissipation coefficient b^* are considered. From the point of view of isolation efficiency of all wave barriers, it is found that the porosity ϕ is relevant when is near the critical porosity ϕ_{cr} and the dimensionless dissipation coefficient is $b^* < 5$. Also, results do not vary

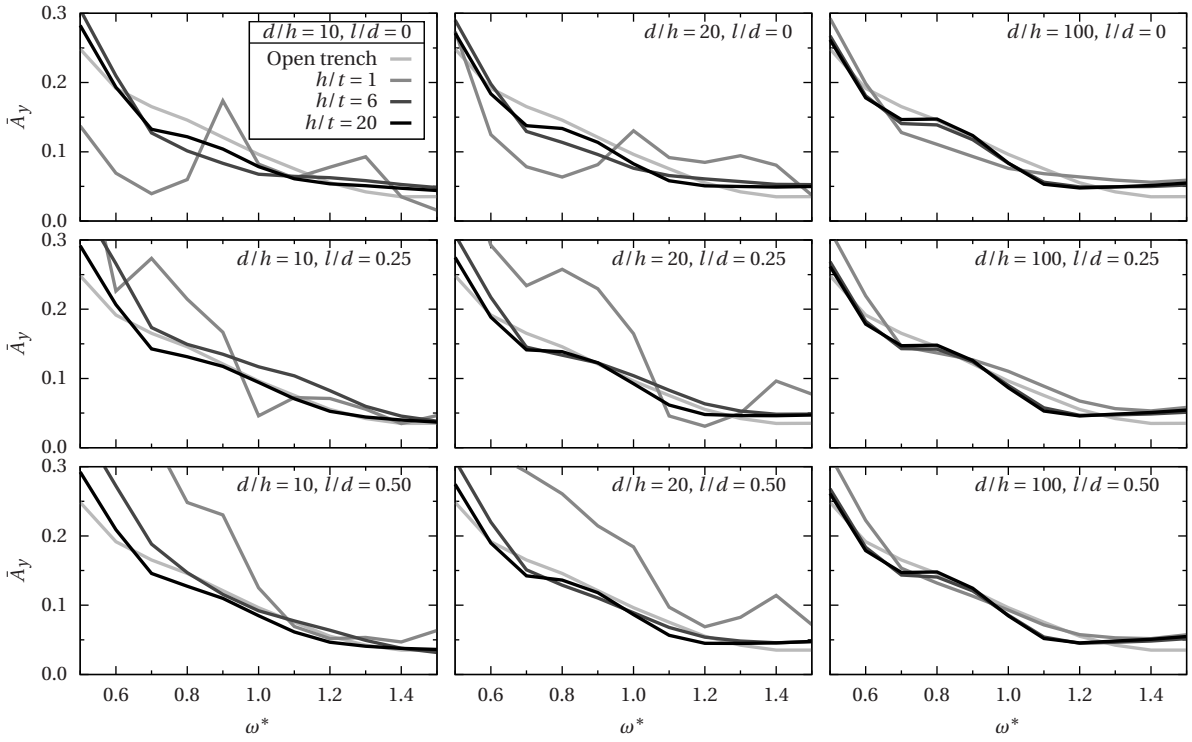

Figure 10: $\bar{A}_y$ comparison between open trench and open trench-wall for different d/h, l/d and h/t ratios ($\phi = 0.20$, $b^* = 0.2$, $\nu_s = 0.30$, $d/w = 2$)

significantly beyond $b^* > 5$, and Poisson's ratio ν_s becomes relevant only for dimensionless frequency $\omega^* < 0.8$. Qualitatively, the open trench and the simple wall (thin in-filled trench) behave similarly to those in elastic soils, except for high porosities and small dimensionless dissipation coefficients. For the evaluation of the isolation efficiency of an open trench-wall, it is found that the influence of the walls can be ignored if they are typical sheet piles, and if the dimensionless frequency ω^* lies between 0.5 and 1.5. This is not the case when walls with bigger cross-sections are used, leading in general to an efficiency loss. Wall burial depths $l/d > 0$ lead to efficiency losses, especially for high porosities and low dimensionless frequencies $\omega^* < 1$.

Acknowledgements

This work was supported by the Subdirección General de Proyectos de Investigación of the Ministerio de Economía y Competitividad (MINECO) of Spain and FEDER through research project BIA2010-21399-C02-01 and also by the Agencia Canaria de Investigación, Innovación y Sociedad de la Información (ACIISI) of the Government of the Canary Islands and FEDER through research project ProID20100224. J.D.R. Bordón was recipient of the fellowship TESIS20120051 from the Program of predoctoral fellowships of the ACIISI until September 2014, and currently is recipient of the research fellowship FPU13/01224 from the Ministry of Education, Culture and Sports of Spain. The authors are grateful for this support.

A Fundamental solution matrices $\mathbf{T}^*$, $\mathbf{D}^*$ and $\mathbf{S}^*$

Elements of the fundamental solution matrix $\mathbf{T}^*$:

$$U^*_{n00} + JX'^*_j n_j = \frac{1}{2\pi} W_0 \frac{\partial r}{\partial n} \tag{54}$$

$$W_0 = \left(Z\Theta - J\frac{\partial \eta}{\partial r} \right) \tag{55}$$

$$t^*_{0k} = \frac{1}{2\pi} \left[T_{01} r_{,k} \frac{\partial r}{\partial n} + T_{02} n_k \right] \tag{56}$$

$$T_{01} = -2\mu \left(\frac{\partial \Theta}{\partial r} - \frac{1}{r}\Theta \right) \tag{57}$$

$$T_{02} = -\lambda \left(\frac{\partial \Theta}{\partial r} + \frac{1}{r}\Theta \right) - 2\mu \frac{1}{r}\Theta + \frac{Q}{R}\eta \tag{58}$$

$$U^*_{nl0} = \frac{1}{2\pi\mu}\left[W_1 r_{,l}\frac{\partial r}{\partial n} + W_2 n_l\right] \tag{59}$$

$$W_1 = Z\chi - \mu\left(\frac{\partial\Theta}{\partial r} - \frac{1}{r}\Theta\right) \tag{60}$$

$$W_2 = -Z\psi - \mu\frac{1}{r}\Theta \tag{61}$$

$$t^*_{lk} = \frac{1}{2\pi}\left[T_1 r_{,l} r_{,k}\frac{\partial r}{\partial n} + T_2\left(\frac{\partial r}{\partial n}\delta_{lk} + r_{,k}n_l\right) + T_3 r_{,l} n_k\right] \tag{62}$$

$$T_1 = -2\left(\frac{\partial\chi}{\partial r} - \frac{2}{r}\chi\right) \tag{63}$$

$$T_2 = \frac{\partial\psi}{\partial r} - \frac{1}{r}\chi \tag{64}$$

$$T_3 = \frac{\lambda}{\mu}\left(\frac{\partial\psi}{\partial r} - \frac{\partial\chi}{\partial r} - \frac{1}{r}\chi\right) - \frac{2}{r}\chi + \frac{Q}{RJ}\Theta \tag{65}$$

Elements of the fundamental solution matrix $\mathbf{D}^*$:

$$d^*_{00} = \frac{1}{2\pi J} W_0 \frac{\partial r}{\partial n^i} \tag{66}$$

$$d^*_{0k} = \frac{1}{2\pi\mu}\left(-W_1 r_{,k}\frac{\partial r}{\partial n^i} + W_2 n^i_k\right) \tag{67}$$

$$d^*_{l0} = \frac{1}{2\pi J}\left(-T_{01} r_{,l}\frac{\partial r}{\partial n^i} + T_{02} n^i_l\right) \tag{68}$$

$$d^*_{lk} = \frac{1}{2\pi}\left[T_1 r_{,l} r_{,k}\frac{\partial r}{\partial n^i} - T_2\left(-\frac{\partial r}{\partial n^i}\delta_{lk} + r_{,l}n^i_k\right) - T_3 r_{,k} n^i_l\right] \tag{69}$$

Elements of the fundamental solution matrix $\mathbf{S}^*$:

$$s^*_{00} = \frac{1}{2\pi}\left[Q_1\frac{\partial r}{\partial n}\frac{\partial r}{\partial n^i} + Q_2 n_j n^i_j\right] \tag{70}$$

$$Q_1 = \frac{Z^2}{\mu}\chi - 2Z\left(\frac{\partial\Theta}{\partial r} - \frac{1}{r}\Theta\right) + J\left(\frac{\partial^2\eta}{\partial r^2} - \frac{1}{r}\frac{\partial\eta}{\partial r}\right) \tag{71}$$

$$Q_2 = \frac{Z^2}{\mu}\psi + 2Z\frac{1}{r}\Theta - J\frac{1}{r}\frac{\partial\eta}{\partial r} \tag{72}$$

$$s^*_{0k} = \frac{1}{2\pi}\left\{S_{01} r_{,k}\frac{\partial r}{\partial n}\frac{\partial r}{\partial n^i} + S_{02} n_k\frac{\partial r}{\partial n^i} + S_{03}\left[n^i_k\frac{\partial r}{\partial n} + r_{,k} n_j n^i_j\right]\right\} \tag{73}$$

$$S_{01} = -2Z\left(\frac{\partial\chi}{\partial r} - \frac{2}{r}\chi\right) - 2\mu\left[-\frac{\partial^2\Theta}{\partial r^2} + \frac{3}{r}\left(\frac{\partial\Theta}{\partial r} - \frac{1}{r}\Theta\right)\right] \tag{74}$$

$$\begin{aligned} S_{02} = {} & Z\left[\frac{\lambda}{\mu}\left(\frac{\partial\psi}{\partial r} - \frac{\partial\chi}{\partial r} - \frac{1}{r}\chi\right) - \frac{2}{r}\chi\right] + \lambda\left[\frac{\partial^2\Theta}{\partial r^2} + \frac{1}{r}\left(\frac{\partial\Theta}{\partial r} - \frac{1}{r}\Theta\right)\right] \\ & + 2\mu\frac{1}{r}\left(\frac{\partial\Theta}{\partial r} - \frac{1}{r}\Theta\right) + \frac{Q}{RJ}\left(Z\Theta - J\frac{\partial\eta}{\partial r}\right) \end{aligned} \tag{75}$$

$$S_{03} = -Z\left(\frac{\partial\psi}{\partial r} - \frac{1}{r}\chi\right) - 2\mu\frac{1}{r}\left(\frac{\partial\Theta}{\partial r} - \frac{1}{r}\Theta\right) \tag{76}$$

$$s^*_{l0} = \frac{1}{2\pi}\left\{-S_{01} r_{,l}\frac{\partial r}{\partial n}\frac{\partial r}{\partial n^i} + S_{02} n^i_l\frac{\partial r}{\partial n} - S_{03}\left[-n_l\frac{\partial r}{\partial n^i} + r_{,l} n_j n^i_j\right]\right\} \tag{77}$$

$$\begin{aligned} s^*_{lk} = {} & \frac{\mu}{2\pi}\left\{S_1\left[r_{,l} n^i_k\frac{\partial r}{\partial n} - r_{,k} n_l\frac{\partial r}{\partial n^i} - \frac{\partial r}{\partial n}\frac{\partial r}{\partial n^i}\delta_{lk} + r_{,k} r_{,l} n_j n^i_j\right]\right. \\ & + S_2\left(r_{,k} n^i_l\frac{\partial r}{\partial n} - r_{,l} n_k\frac{\partial r}{\partial n^i}\right) + S_3 r_{,l} r_{,k}\frac{\partial r}{\partial n}\frac{\partial r}{\partial n^i} \\ & \left. + S_4\left[n_j n^i_j\delta_{lk} + n_l n^i_k\right] + S_5 n_k n^i_l\right\} \end{aligned} \tag{78}$$

$$S_1 = -\frac{\partial^2\psi}{\partial r^2} + \frac{1}{r}\left(\frac{\partial\psi}{\partial r} + 3\frac{\partial\chi}{\partial r} - \frac{6}{r}\chi\right) \tag{79}$$

$$S_2 = 2\frac{\lambda}{\mu}\left[-\frac{\partial^2\psi}{\partial r^2} + \frac{\partial^2\chi}{\partial r^2} + \frac{1}{r}\left(\frac{\partial\psi}{\partial r} - \frac{2}{r}\chi\right)\right] + \frac{4}{r}\left(\frac{\partial\chi}{\partial r} - \frac{2}{r}\chi\right) - \frac{2Q}{RJ}\left(\frac{\partial\Theta}{\partial r} - \frac{1}{r}\Theta\right) \tag{80}$$

$$S_3 = 4\left[-\frac{\partial^2\chi}{\partial r^2} + \frac{1}{r}\left(5\frac{\partial\chi}{\partial r} - \frac{8}{r}\chi\right)\right] \tag{81}$$

$$S_4 = -\frac{2}{r}\left(\frac{\partial\psi}{\partial r} - \frac{1}{r}\chi\right) \tag{82}$$

$$\begin{aligned} S_5 = {} & \frac{\lambda^2}{\mu^2}\left[-\frac{\partial^2\psi}{\partial r^2} + \frac{\partial^2\chi}{\partial r^2} + \frac{1}{r}\left(-\frac{\partial\psi}{\partial r} + 2\frac{\partial\chi}{\partial r}\right)\right] - \frac{\lambda}{\mu}\frac{4}{r}\left(\frac{\partial\psi}{\partial r} - \frac{\partial\chi}{\partial r} - \frac{1}{r}\chi\right) + \frac{4}{r^2}\chi \\ & + \frac{Q}{R}\frac{1}{J}\left[-2\frac{\lambda}{\mu}\left(\frac{\partial\Theta}{\partial r} + \frac{1}{r}\Theta\right) - \frac{4}{r}\Theta + \frac{Q}{R\mu}\eta\right] \end{aligned} \tag{83}$$

References

[1] J. D. Achenbach. *Wave propagation in elastic solids*, volume 16 of *Applied mathematics and mechanics*. North-Holland, 1973.

[2] S. Ahmad and T. M. Al-Hussaini. Simplified design for vibration screening by open and in-filled trenches. *Journal of Geotechnical Engineering*, 117:67–88, 1991.

[3] L. Andersen and S. R. K. Nielsen. Reduction of ground vibration by means of barriers or soil improvement along a railway track. *Soil Dynamics and Earthquake Engineering*, 25:701–716, 2005.

[4] J. Avilés and F. J. Sánchez-Sesma. Foundation isolation from vibrations using piles as barriers. *Journal of Engineering Mechanics*, 114:1854–1870, 1988.

[5] P. K. Banerjee, S. Ahmad, and K. Chen. Advanced application of BEM to wave barriers in multi-layered three-dimensional soil media. *Earthquake Engineering and Structural Dynamics*, 16:1041–1060, 1988.

[6] D. D. Barkan. *Dynamics of bases and foundations*. McGraw-Hill Book Company, Inc., 1962.

[7] J. G. Berryman. Confirmation of Biot's theory. *Applied Physics Letters*, 37(4):382–384, 1980.

[8] D. E. Beskos, B. Dasgupta, and I. G. Vardoulakis. Vibration isolation using open or filled trenches. Part 1: 2-D homogeneous soil. *Computational Mechanics*, 1:43–63, 1986.

[9] M. A. Biot. Theory of propagation of elastic waves in a fluid-saturated porous solid. I. Low-frequency range. *Journal of Acoustical Society of America*, 28(2):168–178, 1956.

[10] J. D. R. Bordón, J. J. Aznárez, and O. Maeso. A 2D BEM-FEM approach for time harmonic fluid-structure interaction analysis of thin elastic bodies. *Engineering Analysis with Boundary Elements*, 43:19–29, 2014.

[11] Y. Q. Cai, G. Y. Ding, and C. J. Xu. Amplitude reduction of elastic waves by a row of piles in poroelastic soil. *Computers and Geotechnics*, 36:463–473, 2009.

[12] Y. Q. Cai, G. Y. Ding, C. J. Xu, and J. Wang. Vertical amplitude reduction of Rayleigh waves by a row of piles in a poroelastic half-space. *International Journal for Numerical and Analytical Methods in Geomechanics*, 33:1799–1821, 2009.

[13] Z. Cao and Y. Q. Cai. Isolation of train-induced ground-borne vibration by trenches on a poroelastic half-space. *Journal of Engineering Mechanics*, 139:580–593, 2013.

[14] F. Chirino and R. Abascal. Dynamic and static analysis of cracks using the hypersingular formulation of the boundary element method. *International Journal for Numerical Methods in Engineering*, 43:365–388, 1998.

[15] B. Dasgupta, D. E. Beskos, and I. G. Vardoulakis. Vibration isolation using open or filled trenches. Part 2: 3-D homogeneous soil. *Computational Mechanics*, 6:129–142, 1990.

[16] H. Deresiewicz. The effect of boundaries on wave propagation in a liquid-filled porous solid: IV. Surface waves in a half-space. *Bulletin of the Seismological Society of America*, 52(3):627–638, 1962.

[17] J. Domínguez. Boundary element approach for dynamic poroelastic problems. *International Journal for Numerical Methods in Engineering*, 35:307–324, 1992.

[18] J. Domínguez. *Boundary Elements in Dynamics*. International Series on Computational Engineering. Computational Mechanics Publications, 1993.

[19] K. Emad and G. D. Manolis. Shallow trenches and propagation of surface waves. *Journal of Engineering Mechanics*, 111:279–282, 1985.

[20] S. François, M. Schevenels, P. Galvín, G. Lombaert, and G. Degrande. A 2.5D coupled FE-BE methodology for the dynamic interaction between longitudinally invariant structures and a layered halfspace. *Computer Methods in Applied Mechanics and Engineering*, 199:1536–1548, 2010.

[21] R. Gallego and J. Domínguez. Hypersingular BEM for transient elastodynamics. *International Journal for Numerical Methods in Engineering*, 39:1681–1705, 1996.

[22] P. Galvín and J. Domínguez. Experimental and numerical analyses of vibrations induced by high-speed trains on the Córdoba–Málaga line. *Soil Dynamics and Earthquake Engineering*, 29:641–657, 2009.

[23] H.-K Hong and J.T. Chen. Derivations of integral equations of elasticity. *Journal of Engineering Mechanics*, 114(6):1028–1044, 1988.

[24] S. E. Kattis, D. Polyzos, and D. E. Beskos. Vibration isolation by a row of piles using a 3-D frequency domain BEM. *International Journal for Numerical Methods in Engineering*, 46:713–728, 1999.

[25] V. D. Kupradze. *Three-dimensional problems of the mathematical theory of elasticity and thermoelasticity*, volume 25 of *Applied mathematics and mechanics*. North-Holland, 1979.

[26] K. L. Leung, D. E. Beskos, and I. G. Vardoulakis. Vibration isolation using open of filled trenches: Part 3: 2-D non-homogenous soil. *Computational Mechanics*, 7:137–148, 1990.

[27] C. H. Lin, V. W. Lee, and M. D. Trifunac. The reflection of plane waves in a poroelastic half-space saturated with inviscid fluid. *Soil Dynamics and Earthquake Engineering*, 25:205–223, 2005.

[28] O. Maeso, J. J. Aznárez, and F. García. Dynamic impedances of piles and groups of piles in saturated soils. *Computers and Structures*, 83:769–782, 2005.

[29] P. A. Martin, F. J. Rizzo, and T. A. Cruse. Smoothness-relaxation strategies for singular and hypersingular integral equations. *International Journal for Numerical Methods in Engineering*, 42:885–906, 1998.

[30] L. A. Padrón, J. J. Aznárez, and O. Maeso. BEM-FEM coupling model for the dynamic analysis of piles and pile groups. *Engineering Analysis with Boundary Elements*, 31:473–484, 2007.

[31] A. Portela, M. H. Aliabadi, and D. P. Rooke. The dual boundary element method: effective implementation for crack problems. *International Journal for Numerical Methods in Engineering*, 33:1269–1287, 1992.

[32] A. Sáez, R. Gallego, and J. Domínguez. Hypersingular quarter-point boundary elements for crack problems. *International Journal for Numerical Methods in Engineering*, 38:1681–1701, 1995.

[33] P. H. Tsai and T. S. Chang. Effects of open trench siding on vibration-screening effectiveness using the two-dimensional boundary element method. *Soil Dynamics and Earthquake Engineering*, 29:865–873, 2009.

[34] R. D. Woods. *Screening of elastic surface waves by trenches*. PhD thesis, University of Michigan, 1967.

[35] B. Xu, J. F. Lu, and J. H. Wang. Numerical analysis of the isolation of the vibration due to Rayleigh waves by using pile rows in the poroelastic medium. *Archive of Applied Mechanics*, 80:123–142, 2010.

[36] J. Yang. A note on Rayleigh wave velocity in saturated soils with compressible constituents. *Canadian Geotechnical Journal*, 38(6):1360–1365, 2001.